INFACON 7, Trondheim, Norway, June 1995
Eds.: Tuset, Tveit and Page
Publishers: FFF, Trondheim, Norway

RELATIONSHIPS BETWEEN THE GRINDING BEHAVIOUR AND THE MICROSTRUCTURE OF FERRO-SILICON ALLOYS WITH 65 WT. % SILICON

C. Guéneau*°, C. Servant°, F. Manier*

* Laboratoire Central de Recherches de Chedde, Péchiney Electrométallurgie (PEM), 74190 Le Fayet, France.

° Laboratoire de Métallurgie Structurale, URA CNRS 1107, Bât. 413, Université de Paris-Sud, 91405 Orsay Cedex, France.

ABSTRACT

During the grinding process, ferro-silicon alloys with 65 wt. % Si produce an important quantity of undesirable fines. The presence of a crack net in the $Si_{2.4}Fe$ matrix in the bulk material was found to be responsible for this fine production, the size of the grains delineated by the cracks being very close to the one of the fines (several hundred microns). In the case of the two-phase alloys, the cracking initiation would be induced by thermomechanical stresses due to the difference between dilation coefficients of silicon and $Si_{2.4}Fe$ during the alloy cooling. When the silicon content increases, the fine production decreases as well as the $Si_{2.4}Fe$ volume fraction. Among the alloying elements, only calcium addition is favourable. In fact, calcium precipitates as Si_2Ca plates which prevent the crack spreading in the matrix. Moreover, the fine production is slowed down by an increasing cooling rate, providing a smaller silicon grain size, then extending the barrier to the crack spreading.The knowledge of the major parameters influencing the grinding behaviour have enabled a better control of the ferro-silicon alloy production.

INTRODUCTION

Industrial ferro-silicon alloys containing 65 wt. % Si are used as cast-iron inoculants in the production of steel or high purity ferro-silicon magnetic sheets. The alloys, produced by the PEM Society, are obtained from silica and scrap iron with carbon as the reducing agent in electric arc furnaces. The material contains a number of alloying elements, particularly aluminium and calcium, but also manganese, zirconium and titanium. During the grinding process of ferro-silicon ingots, a very important quantity of fines is produced. This paper aims at understanding this grinding behaviour by relating the microstructure and the mechanical properties of ferro-silicon. Different parameters were taken into account such as the silicon content, the nature and the amount of the alloying elements and the ingot cooling rate. A high purity two-phase alloy with 65 wt. % Si was chosen as a reference. Model ferro-silicon alloys were prepared in order to study the respective influence of these parameters.

MATERIALS

In Table 1 are given all the considered alloys as a function of the parameters involved.

Parameter	Alloy designation	
Silicon content	65HP reference 75HP	HP: high purity medium cooling rate
Cooling rate	65HPL 65HPVL 65HPF 1.5ALF	L: low cooling rate (50°C/h) VL: very low cooling rate (10°C/h) F: fast cooling rate
Alloying element (wt. %)	1AL 1.5AL 4AL 1CA 1.8CA 4CA 4MN 4ZR	silicon content: 65 wt. % same cooling rate as 65HP

TABLE 1. Alloy classification as a function of the studied parameters.

The 65HP reference material was an industrial high purity alloy with 65 wt. % silicon. The ternary alloys have been prepared by melting the 65HP reference industrial alloy in which the pure alloying element was added. Concerning the solidification parameter, different cooling rates were considered: slow rates by controlling the furnace heat treatment program and fast rates by modifying the ingot thickness. In Table 2, the alloy chemical analysis are listed.

Alloy designation	Si (wt. %)	Fe (wt. %)	Ca (wt. %)	Al (wt. %)	Mn (wt. %)	Zr (ppm)
65HP	64.6	34.2	0.073	0.12	0.12	8
75HP	75.9	23.9	0.017	0.008	0.09	-
1AL	66.1	31.8	0.15	0.96	0.11	7
1.5AL	65.1	32.0	0.078	1.53	0,11	6
4AL	64.9	30.7	0.05	4.11	0.13	18
1CA	65.8	32.1	0.6	0.02	0.11	14
1.8CA	65.1	32.1	1.25	0.024	0.11	8
4CA	65.3	29.8	4.27	0.2	0.16	67
4MN	64.4	31.2	0.02	0.022	4.08	350
4ZR	65.5	30.3	0.15	0.022	0.12	3.65*

TABLE 2. Alloy chemical analysis (*: in wt. %).

EXPERIMENTAL AND CALCULATION METHODS

MICROSTRUCTURE

The alloy microstructure was observed by optical and scanning electron microscopy. The phase composition was measured with an electron microprobe. The phase volume percentages were determined by four methods:
- chemical analysis [1];

- thermodynamic calculations [2]; all ternary phase diagrams were derived from a thermodynamic calculation using the least-squares optimization programs of Lukas et al [3] and PARROT, available in Thermo-Calc software [4,5,6,7]. The phase mole fraction at equilibrium can be calculated at any temperature and for any overall composition of these alloys;
- nuclear neutron diffraction experiments. These experiments were made on powder specimens with a high resolution diffractometer (λ=2.426Å). The Rietveld profile refinement procedure was used to calculate the phase volume fraction by fitting the calculated spectra to the experimental data [1]. Previously, it was necessary to determine the crystalline structure of some intermetallic compounds such as $FeAl_3Si_2$ and $Fe_2Al_3Si_3$ by X-ray diffraction [8,9];
- image analysis; this method was applied on back-scattered electron images treated by the Optilab program.

GRINDING SIMULATION

In order to increase the grinding productivity and the quality of the material, the PEM Society has developed a grindability test and a model to simulate the existing industrial grinding process. The different procedures used are given in Table 3:

Procedure	Input grain size (mm)	Chosen grain size (mm)	Fine size (mm)
A: coarse grinding	0-20	0-5	<0.2
B: fine grinding	0-80	0-2	<0.2
C: fine grinding	0-2	0-0.5	<0.2

TABLE 3. Considered grinding procedures.

Most studies about simulation are mainly based on comminution energy concerning ball mills in terms of size distribution process [10,11,12,13]. PEM model allows the prediction of particle size distribution and flowrate in case of roller mills, hammer mills, jaw crushers, giratory crushers, screens and separators. It is based on the knowledge of crushers and products. The intrinsic grinding behaviour of the product is independant of the crusher and statiscally, the grinding of one particle gives the same size distribution whatever the mill is, as the applied energy is in the same range value. The mathematic representation of the grinding behaviour is a matrix called "grinding matrix", determined by a "grindability test" using a 5 tons press. A grain single-layer with a fixed size range is crushed between two plates; the size distribution result, measured by screening, leads to the calculation of one column of the grinding matrix. This test is made with four size ranges in mm: 16/20, 8/10, 4/5, 2/2.5. The matrix for 80 ranges between 0.01 to 100 mm is determined by extrapolation. The crusher model uses the following parameters: flowrate, opening, feed size distribution, which depend on the type of crusher. It leads to the calculation of the selecting function which gives the percentage of ground or not ground particles. The screen model gives the overflow and underflow solid flowrates and size distribution. The simulation ouputs are size distribution and flowrate.

The grindability test results are not presented in the present paper because they do not show a significant evolution as a function of the different studied alloys. In the case of the cooling rate parameter, the grindability tests have not been carried out because of the too low available quantity of material. So, the grinding simulation was not possible. However, the microstructure of the alloys cooled with different cooling rates has been studied and will be discussed later.

RESULTS AND DISCUSSION

The iron-silicon phase diagram is given in Figure 1.

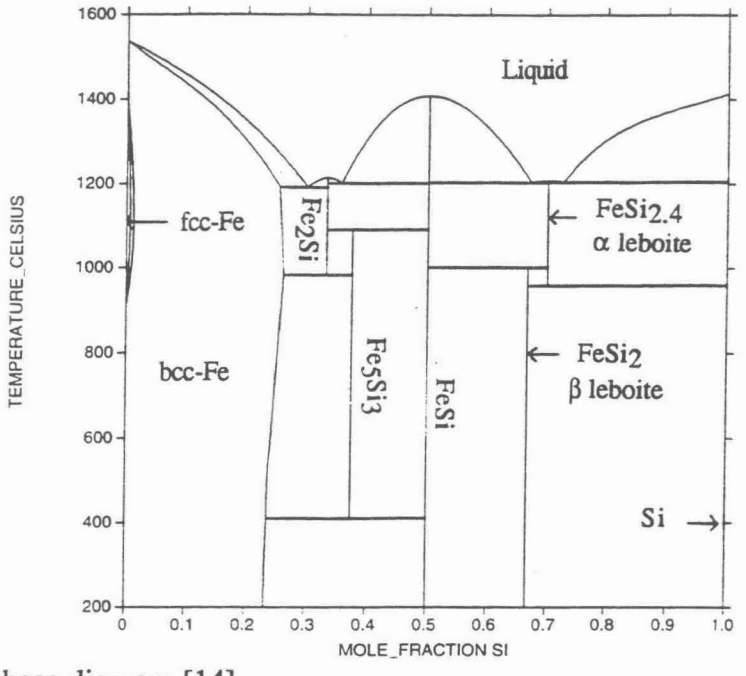

FIG.1. Iron-silicon phase diagram [14].

All the studied alloys are constituted of silicon plates in a $Si_{2.4}Fe$ leboite matrix. The fast cooling rate does not enable the eutectoid transformation ($Si_{2.4}Fe$ -> $0.4Si+Si_2Fe$) to occur. Figure 2 shows the evolution of the percentage of fines for the A grinding procedure as a function of the silicon content for two-phase alloys (from 60 to 80 wt. % Si) as well as for single-phase materials silicon and $Si_{2.4}Fe$.

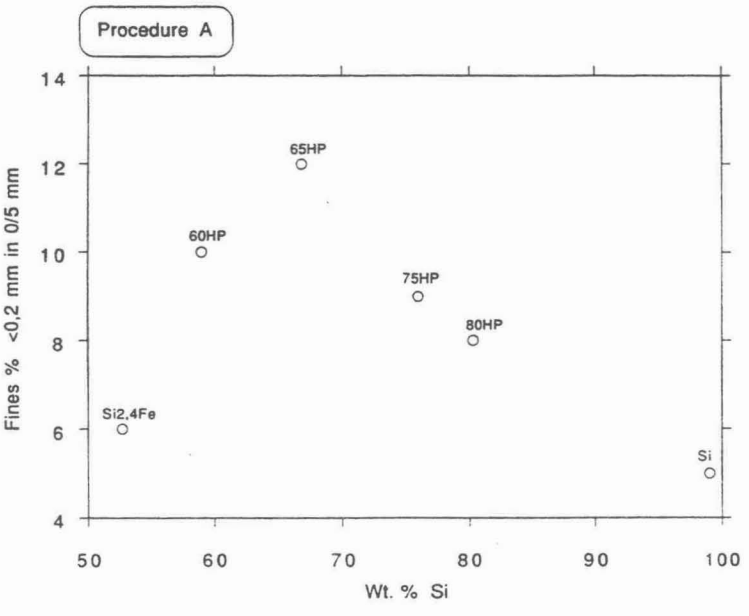

FIG. 2. Fine percentage as a function of the silicon content for two-phase alloys and single-phase materials for the simulation of the A grinding procedure.

The two single-phase materials produce the lowest fine quantity while all the two-phase alloys exhibit a higher significant production of fines, which can be twice as important as in the single-phase materials (about 10 %). Except for the 60HP alloy, the fine percentage decreases as the silicon content is increasing.

Figure 3 shows the evolution of the fine percentage for the alloys containing alloying elements as a function of the grinding procedure and the silicon content.

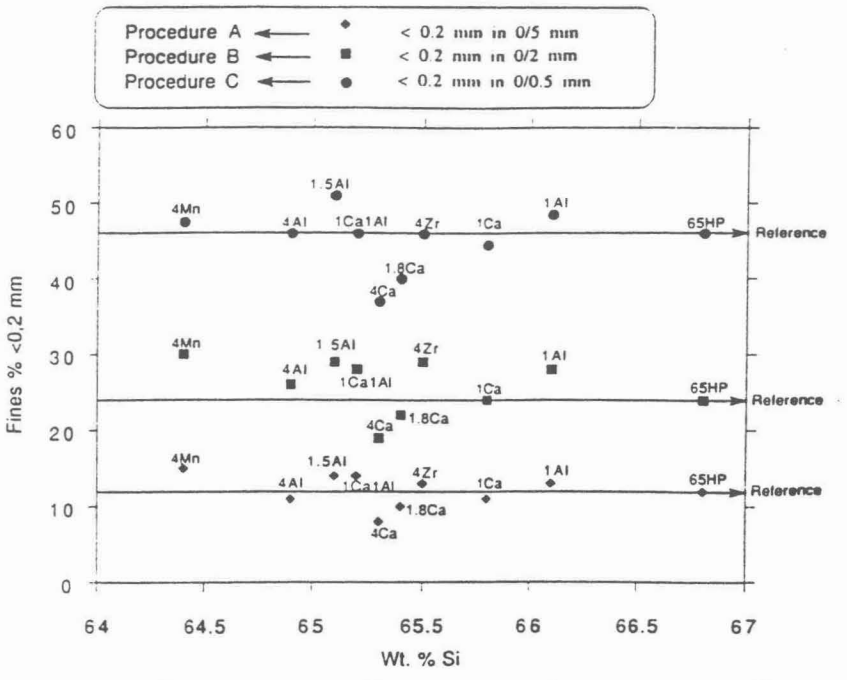

FIG.3. Fine percentage as a function of the silicon content for the A,B and C procedures for ferro-silicon containing an alloying element.

The comparison of both figures 2 and 3 shows that in general, for the A coarse grinding process, the ferro-silicon with alloying element exhibit a worse grinding behaviour than the binary alloys, except the 1.8CA and 4CA samples. For the B and C finest grinding procedures, the fine quantity increases as expected, up to 50 %. The grinding behaviour of all the studied alloys is about the same for the different procedures. Among the alloying elements, calcium is able to improve the grinding behaviour of ferro-silicon as compared to the 65HP reference. Moreover, an increasing calcium amount is favourable. On the contrary, aluminium, manganese and zirconium additions do not exhibit a better behaviour and can be undesirable.

Figure 4 shows the microstructure of the 65HP alloy.

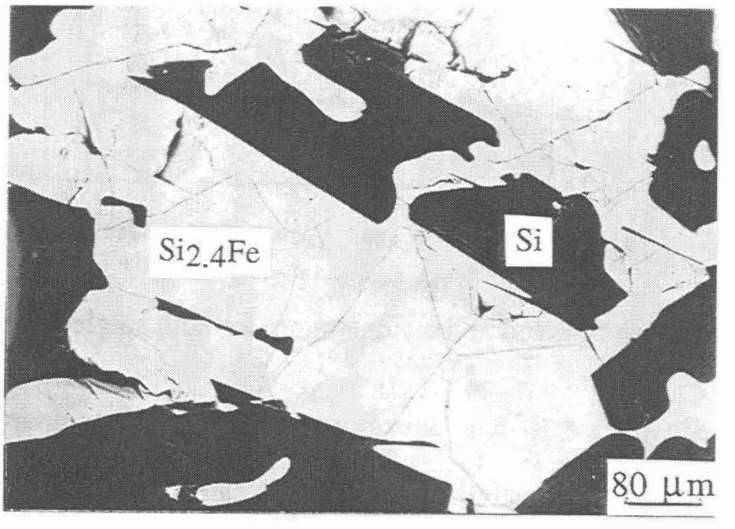

FIG.4. Back-scattered electron micrograph of the 65HP alloy showing the crack net in the $Si_{2.4}Fe$ matrix.

In this alloy, a crack net was observed in the $Si_{2.4}Fe$ matrix as well as in all two-phase alloy ingots. Moreover, it seems that the crack spreading is stopped at the $Si/Si_{2.4}Fe$ interfaces. The size of the grains delineated by the cracks is very close to the grain size of the fines, about several hundred microns (Figure 5), which can explain the important amount of the fine production.

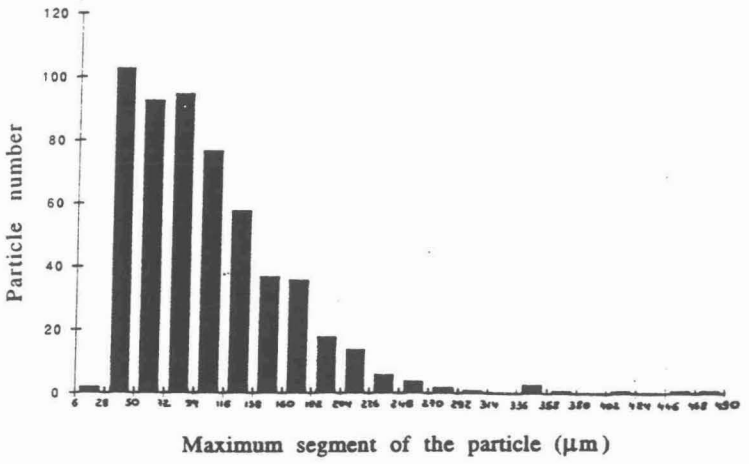

FIG.5. Size distribution of the grains delineated by the cracks in the matrix of the 65HP alloy.

No cracks were found in silicon plates. In addition, no net of cracks was observed in the pure Si2.4Fe phase; this signifies that the cracks are induced by thermomechanical stresses, resulting from the difference of behaviour between the two pure phases during the solidification process. Thermal dilation coefficients of pure silicon and Si2.4Fe phases and of the 65HP reference alloy have been measured during the following heat treatment: heating up to 1100°C and cooling to room temperature, performed with a rate of 300°C/h (Figure 6).

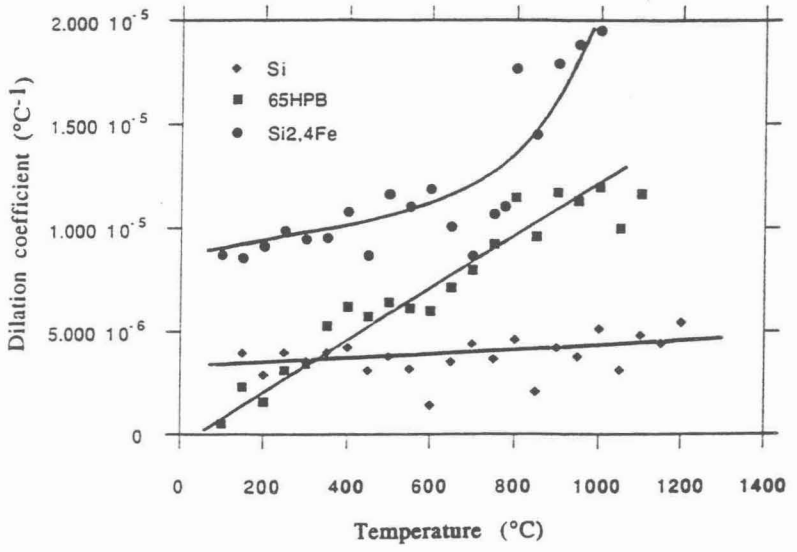

FIG.6. Dilation coefficients as a function of the temperature for both single-phase material and the 65HP alloy.

It will be noted that the Si2.4Fe matrix contracts more twice to fourth compared to pure silicon. This difference may account for the matrix cracking. In fact, in silicon plates, the cracks are in compression while in the matrix, they are in tensile and so can spread over in the material. The shape of the crack net can be explained by the isotropic silicon plate distribution which delimite the Si2.4Fe volumes. Furthermore, other cracking origines can be considered: on the one hand, the matrix grain boundary fragilisation due to impurity segregation or to the anisotropy of the thermal coefficients of the matrix, having a tetragonal crystalline structure. On the other hand, the no classical behaviour of silicon: its volume increases when it solidifies. The first hypothesis was discarded; in fact, the observation of the material, by scanning electron microscopy using back-scattered electrons at low voltage, showed that the cracks do not coincide with the grain

boundaries. The second hypothesis was also rejected; indeed, the primary silicon solidification occurs into the liquid phase and then does not give rise to stresses. Otherwise, silicon dilation during solidification can play a secondary role during the eutectic reaction (liquid -> Si+$Si_{2.4}Fe$). Most authors quoted the eutectoid transformation ($Si_{2.4}Fe$->Si_2Fe+0.4Si) to be responsible for the cracking matrix because of the leboite crystalline transformation. As it does not take place in our samples, except for the very slow cooling, this factor has been rejected [15-20].

A tentative thermomechanical model was proposed to predict the matrix cracking or not as a function of the alloy cooling rate and the silicon content [1]. In this one-dimensional two beam model, we considered that both pure phases, maintained between two fixed beams (symbolizing the ingot mould inner surfaces), are submitted to both thermal and elastic stresses. The comparison of the resulting calculated stress in the $Si_{2.4}Fe$ with the critical one, determined from the $Si_{2.4}Fe$ toughness could allow to forecast the matrix cracking or not. Calculation from this model needed the determination of the toughness and the Young modulus of both phases. The excessive fragility of the $Si_{2.4}Fe$ phase did not allow these determinations. However, a creep experiment was carried out on the 65HP alloy, using a low stress, in order to measure the cracking temperature. During the alloy solidification, a weak continuous dilation of the sample was observed from about 600°C down to room temperature; in this temperature range, it has been verified that the creep material was negligible. So, the cracking onset was associated with this dilation, starting at about 600-700°C. Further experiments ought to be made to confirm this result.

By taking into account the above analyzed fine origins, the influence of the different chemical and processing parameters can be discussed. The decrease of the fine percentage as a function of the silicon content in two-phase alloys is explained by the simultaneous decrease of the $Si_{2.4}Fe$ volume fraction, which contains the crack net. The results for the alloys containing an alloying element are more difficult to interpret. Figure 7 shows the evolution of the fine percentage versus the $Si_{2.4}Fe$ volume fraction for all ternary alloys as well as for the 65HP.

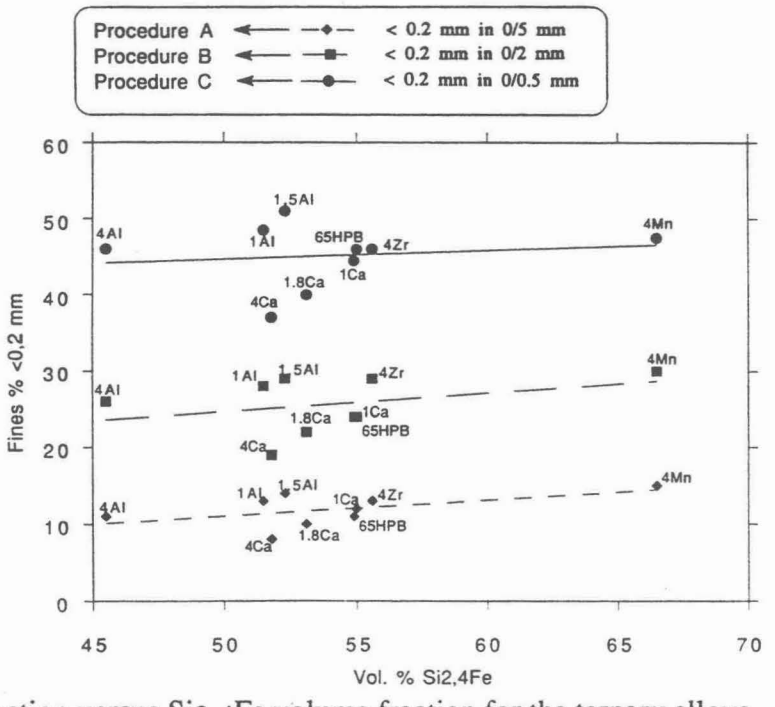

FIG.7. Fine production versus $Si_{2.4}Fe$ volume fraction for the ternary alloys.

This plot presents a slight increase of the fine production with the $Si_{2.4}Fe$ quantity. Furthermore, the discrepancies between the different alloys, referring to 65HP, will be discussed for each alloying element. Plate 1 presents electron micrographs of the 4CA, 4AL, 4MN and 4ZR alloys. Calcium is concentrated in lamellar Si_2Ca precipitates, located in the matrix, orientated perpendicularly to silicon plates. As observed in the micrograph of 4CA, the crack spreading is stopped at the Si_2Ca/$Si_{2.4}Fe$ interfaces, preventing the formation of a real crack net. It seems that

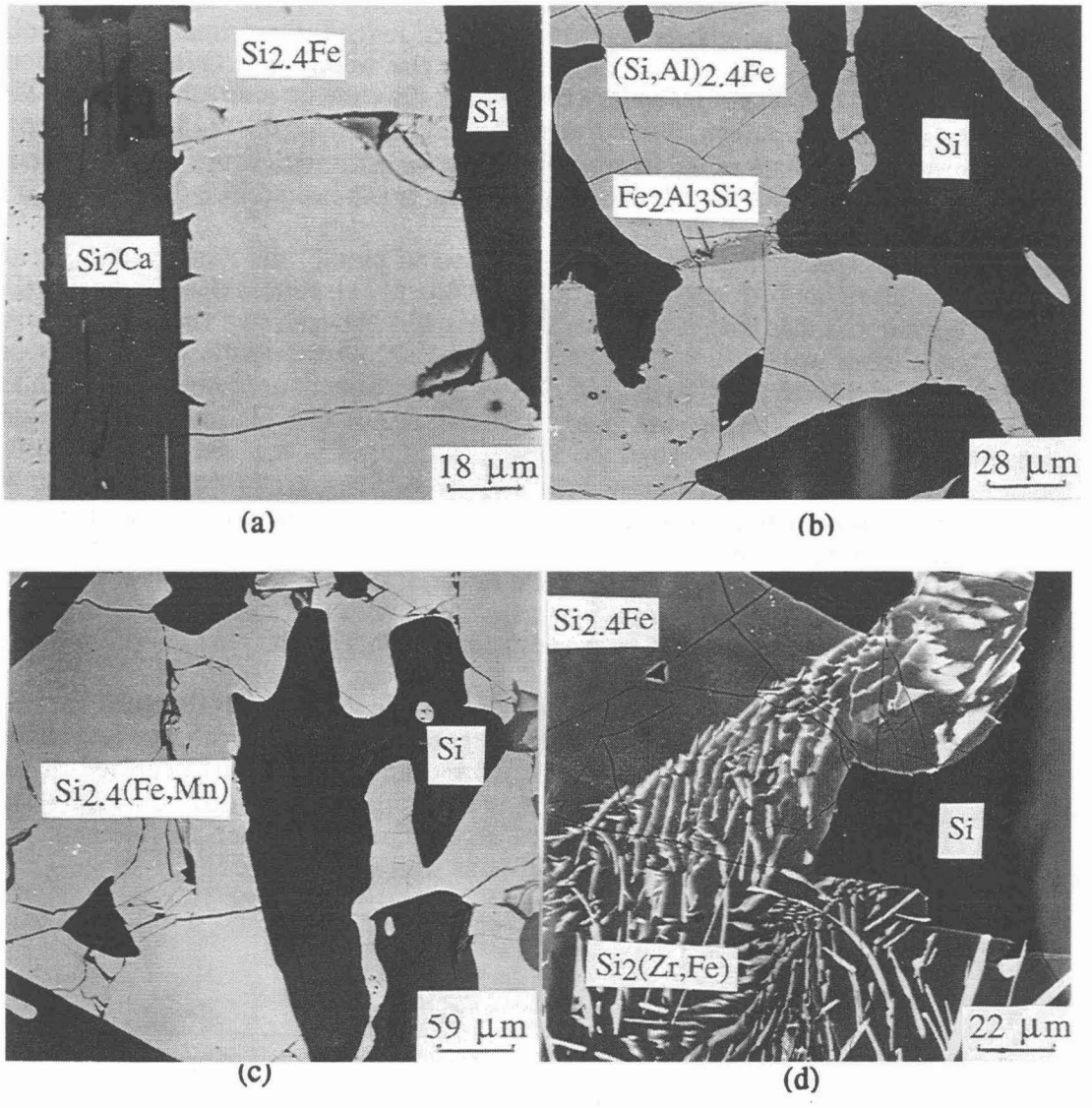

PLATE 1. Electron micrographs of the 4CA (a), 4AL (b), 4MN (c) and 4ZR (d) alloys (with 65 wt. % Si).

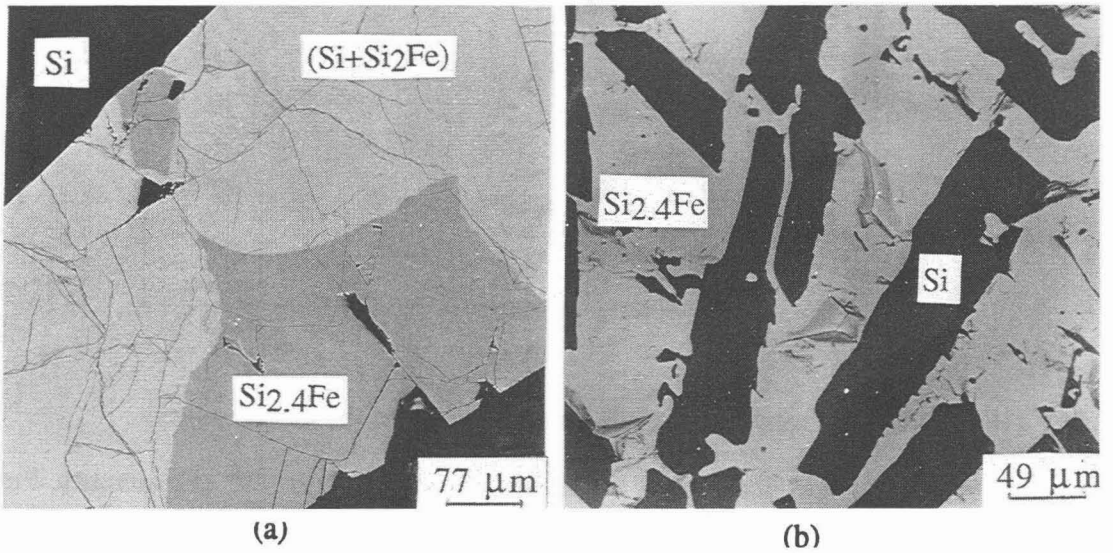

PLATE 2. Electron micrographs of the 65HPVL (a) (very low cooling rate) and 65HPF (b) (fast cooling rate) alloys.

Si_2Ca plays the same role as silicon, blocking the crack spreading in $Si_{2.4}Fe$. So, the decrease in fine production with the calcium content can be both related to the decrease of the $Si_{2.4}Fe$ quantity and to the blocking role of Si_2Ca precipitates. The width of the Si_2Ca plates is increasing with calcium content, reinforcing their blocking role.

Aluminium substitutes for silicon in the matrix and takes part to the formation of both $FeAl_3Si_2$ and $Fe_2Al_3Si_3$ intermetallic compounds. In the 4AL micrograph, it can be seen that these two compounds do not act as cracking barriers. The increasing fine quantity for the 1AL and 1.5AL alloys can be associated with the existence of an aluminium gradient in the matrix, inducing microhardness gradients, so supplementary stresses in the material [21]. As for the 4AL alloy, its better grinding behaviour compared to 1.5AL and 1AL, is due to a less important $Si_{2.4}Fe$ volume fraction.

The 4MN alloy is composed of two phases: silicon and $Si_{2.4}(Fe,Mn)$ where manganese substitutes for iron. This substitution involves a sensible increase of the $Si_{2.4}Fe$ quantity, which may be responsible for the more important fine production, compared to most alloys.

Zirconium is gathered in fine lamellar $Si_2(Zr,Fe)$ precipitates located in the matrix. The micrograph of the 4ZR alloy shows that these precipitates play no blocking role in front of the crack spreading. However, the breaking aspect observation exhibits the taking off of the fine precipitates, which may acts as an unfavourable factor for the material grinding behaviour.

The last studied parameter was the cooling rate (Plate 2). An increase of the cooling rate gives rise to a finer microstructure, with less cracks, which may surprise by considering the stress level increase. But from about 600°C, when the matrix cracking occurs, the cooling rate parameter does not play an important role as the overall microstructure is fixed. The major factor is then the size of the silicon precipitates. In fact, the silicon plate size decreases with an increase of the cooling rate, extending the barrier density in front of the crack spreading in the matrix. These explanations agree with the results of Holdhus [15], Povolotskii et al [19] and Sigfusson et al [20]. On the contrary, a lower cooling rate is not favourable concerning the mechanical behaviour of the material (Plate 2). In fact, a secondary crack net is observed in (Si_2Fe+Si) eutectoid areas, due to volume changes during the crystalline transformation of the leboite. This secondary crack net acts against the strengthening given by the fine silicon eutectoid structure. Therefore, it would be necessary to carry on grinding simulations in order to confirm the influence of this last parameter.

CONCLUSION

The careful study of the alloy microstructure combined with their grinding simulation led to the better understanding of the ferro-silicon fine production. The ways to improve the grinding behaviour of ferro-silicon alloys are the following ones:
- to increase the silicon content in order to decrease the volume fraction of the $Si_{2.4}Fe$ phase and to increase the barrier density to the crack spreading;
- to increase the calcium content, that is to increase the volume fraction of Si_2Ca precipitates, which act as crack spreading barriers;
- to increase the cooling rate in order to diminish the silicon plate size and to avoid the eutectoid transformation to occur.

This analysis may enable a better control of the ferro-silicon elaboration and grinding process.

ACKNOWLEDGEMENTS

The authors would like to thank Professor R. Piques of the Centre des Matériaux de l'Ecole des Mines d'Evry for very helpful discussions about the cracking thermomechanical model and P.H. Galvin of the PEM Society for his great ability concerning the material grinding.

REFERENCES

[1] C.GUENEAU, Thèse de Doctorat en Sciences Physiques, Université de Paris-Sud, (december 1993).

[2] C.GUENEAU, C.SERVANT and I.ANSARA, Journal de Chimie Physique, vol.90, p.409 (1993).

[3] H.L.LUKAS, S.FRIES, U.KATTNER and J.WEISS, Manual of the computer programs, version 91-3, Max Planck Institute, Stuttgart, Germany (August 1991).

[4] B.SUNDMAN, Thermocalc Documentation Set, Division of Physical Metallurgy, Royal Institute of Technology, Stockholm, Sweden (1991).

[5] C.GUENEAU, C.SERVANT and I.ANSARA, Calphad, to be published in vol.3, (1994).

[6] C.SERVANT, C.GUENEAU and I.ANSARA, Journal of Alloys and Compounds, accepted in (february 1994).

[7] C.GUENEAU, C.SERVANT and I.ANSARA, accepted in Proceedings of the TMS Rosemont Symposium, to be published in (1995).

[8] C.GUENEAU, C.SERVANT, F.d'YVOIRE and N.RODIER, Acta Crystallographica, accepted in (june 1994).

[9] C.GUENEAU, C.SERVANT, F.d'YVOIRE and N.RODIER, Acta Crystallographica, to be submitted in (1994).

[10] F.C.BOND, Mining Eng. Transactions of AIME, p.484 (1962).

[11] G.HUYET, Thèse de Doctorat en Sciences, Université de Nancy 1, (June 1974).

[12] J.CHASTANG, H.HUE and A.LAFAYE, Powder Metallurgy, vol.62, p.27, (1990).

[13] J.CARNEL, L'industrie Céramique, vol. 854, p.761, (Nov 1990).

[14] J.C. ANGLEZIO, C. SERVANT and I. ANSARA, Calphad, 18 (3), p.273-302 (1994).

[15] H.HOLDHUS, Journal of The Iron and Steel Institute, vol.200, p.1024, (1962).

[16] J.A. DE HUFF, V.D.COPPOLECCHIA and A.LESNEWICH, Electric Furnace Proceedings, p.167, (1969).

[17] I.N.STRUKOV and P.V.GEL'D, Fizika Metallov I Metallovedenie, vol.3, p.564, (1956).

[18] H.TVEIT, Thesis, NTH Trondheim (1988).

[19] V.D.POVOLOTSKII et al, Izv. V. U. Z. Chernaya Metal., vol.8, p.31, (1987).

[20] I.SIGFUSSON, O.HELGASON, Hyperfine Interactions, vol.54, p.861, (1990).

[21] A.V.SABIRZYANOV and P.V.GEL'D, Trudy Ural. Politekhm. Inst., vol.167, p.75, (1968).